Modular Ion Mobility Calibrants for Organometallic Anions Based on Tetraorganylborate Salts

Thomas Auth,[†,§] Márkó Grabarics,[‡,∥,§] Maria Schlangen,[⊥] Kevin Pagel,*[,‡,∥] and Konrad Koszinowski*[,†]

[†]Institut für Organische und Biomolekulare Chemie, Universität Göttingen, Tammannstraße 2, 37077 Göttingen, Germany

[‡]Institut für Chemie und Biochemie, Freie Universität Berlin, Arnimallee 22, 14195 Berlin, Germany

[∥]Fritz-Haber-Institut der Max-Planck-Gesellschaft, Abteilung Molekülphysik, Faradayweg 4–6, 14195 Berlin, Germany

[⊥]Institut für Chemie, Technische Universität Berlin, Straße des 17. Juni 115, 10623 Berlin, Germany

ABSTRACT: Organometallics are widely used in catalysis and synthesis. Their analysis relies heavily on mass-spectrometric methods, among which traveling-wave ion mobility spectrometry (TWIMS) has gained increasing importance. Collision cross sections (*CCS*) obtainable by TWIMS significantly aid the structural characterization of ions in the gas phase, but for organometallics, their accuracy has been limited by the lack of appropriate calibrants. Here, we propose tetraorganylborates and their alkali-metal bound oligomers $[M_{n-1}(BR_4)_n]^-$ (M = Li, Na, K, Rb, Cs; R = aryl, Et; n = 1–6) as calibrants for electrospray-ionization (ESI) TWIMS. These species chemically resemble typical organometallics and readily form upon negative-ion mode ESI of solutions of alkali-metal tetraorganylborates. By combining different tetraorganylborate salts, we have generated a large number of anions in a modular manner and determined their *CCS* values by drift-tube IMS ($^{DT}CCS_{He}$ = 81–585, $^{DT}CCS_{N2}$ = 130–704 Å^2). In proof-of-concept experiments, we then applied these ^{DT}CCS values to the calibration of a TWIMS instrument and analyzed phenylcuprate and argentate anions, $[Li_{n-1}M_nPh_{2n}]^-$ and $[M_nPh_{n+1}]^-$ (M = Cu, Ag), as prototypical reactive organometallics. The $^{TW}CCS_{N2}$ values derived from TWIMS measurements are in excellent agreement with those determined by drift-tube IMS (< 2% relative difference), demonstrating the effectiveness of the proposed calibration scheme. Moreover, we used theoretical methods to predict the structures and *CCS* values of the anions considered. These predictions are in good agreement with the experimental results and give further insight into the trends governing the assembly of tetraorganylborate, cuprate, and argentate oligomers.

Organometallic compounds and transition-metal catalysts are of outstanding practical importance. Many of these systems show a high degree of complexity because of their propensity to adopt different coordination, aggregation, and oxidation states and to undergo fast intermolecular exchange processes, which renders their analysis challenging.[1-6] Among the most useful methods for analyzing organometallics and transition-metal catalysts is mass spectrometry (MS).[7] Simple MS measurements can afford unambiguous stoichiometric information whereas MS/MS experiments greatly facilitate the characterization by shutting down intermolecular exchange reactions. Accordingly, mass spectrometry and related gas-phase methods play an important role in identifying reactive intermediates as well as determining the stability and reactivity of organometallic compounds.[8-14] These applications have considerably benefitted from the introduction of electrospray ionization (ESI).[15] This ionization technique has significantly extended the range of accessible organometallic analytes and also enabled the analysis of non-covalently bound complexes, which typically do not survive harsher ionization conditions.[16-21]

Despite these assets, conventional mass spectrometry suffers from its inability to furnish detailed structural information or to distinguish isomers. The high interest in structural information on gaseous ions has led to the development of ion spectroscopy[22-25] and ion mobility spectrometry (IMS).[26-29] While both techniques can achieve the goal in quest in combination with computational methods, IMS has the advantage of requiring a simpler apparatus. For this reason, commercial ion mobility-mass spectrometers have been available for more than ten years. Arguably, the most popular type of instruments makes use of the traveling-wave technique (TWIMS).[30-32] This technique does not apply a static field, but propagating electric field waves, which drive the ions through a cell filled with an inert buffer gas (typically N_2). However, the oscillating field also results in a more complex physics of the ion motion.[33,34] Therefore, the measured arrival time of an ion in TWIMS instruments cannot be directly converted into its mobility and collision cross section (*CCS*). Instead, it is common practice to derive ion mobilities and ^{TW}CCS values[35] from a comparison with calibrant ions, whose *CCS*s are known from drift-tube ion mobility spectrometry (DTIMS) experiments.[36,37] Thus, accurate ^{TW}CCS values derived from TWIMS measurements require the application of an appropriate calibrant.

Ideal calibrants for TWIMS should be easily available, stable, and non-toxic. They should have high ionization efficiencies and yield clean and simple mass spectra as well as symmetric and unimodal arrival time distributions (ATDs). In addition, calibrants must cover a wide range of mobilities and *CCS* values to be appli-

cable to ions of various sizes. Finally, the calibrant ions preferably have the same charge state as the analytes of interest and chemically closely resemble the latter.[38-44] These properties are of particular importance for obtaining accurate ^{TW}CCSs from TWIMS experiments, which explains that no universal TWIMS calibrant exists. For instance, the commonly applied calibrant polyalanine has proven to perform well for the TWIMS analysis of other polypeptides,[45] but is not the best choice for the investigation of glycans[40] or lipids.[42]

Although several TWIMS calibrants have been established in recent years (most of them being cationic),[38-42,46-53] none of these were designed for the expressed purpose of analyzing typical organometallics or transition-metal catalysts. Hence, the TWIMS investigation of this class of analytes currently lacks a sound foundation. To address this shortcoming, we here propose easily available tetraorganylborates BR_4^- (Scheme 1) and their alkali-metal-bound oligomers $[M_{n-1}(BR_4)_n]^-$ as ESI-TWIMS calibrants for organometallic anions,[54-59] such as organomagnesates,[60,61] -ferrates,[62,63] -palladates,[64-67] -cuprates,[68-70] and -aluminates.[71,72] Tetraorganylborates resemble typical organometallics, but are much less sensitive toward air and moisture and, therefore, easier to handle.[73-76] Moreover, it has been shown very recently that Li^+-bound dimers and trimers of BPh_4^- can be prepared upon ESI of solutions containing $LiBPh_4$.[77] As these species form spontaneously in a modular manner, a small number of M^+ and BR_4^- building blocks is expected to yield a large variety of gaseous $[M_{n-1}(BR_4)_n]^-$ adducts.

Scheme 1. Tetraorganylborates considered in this work

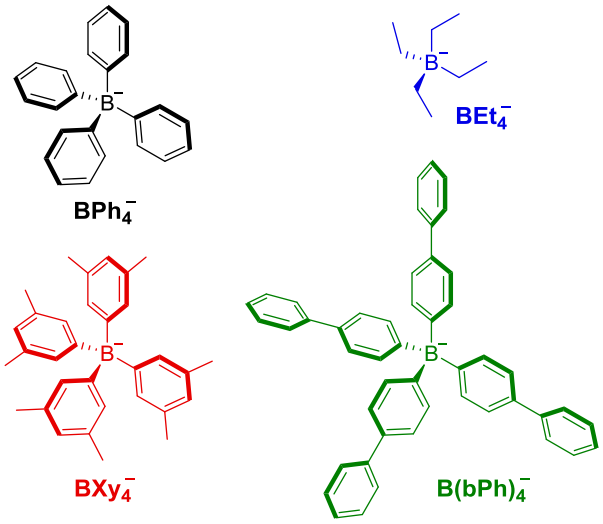

In the present study, we use DTIMS measurements to determine mobilities and absolute ^{DT}CCS values for BR_4^- and $[M_{n-1}(BR_4)_n]^-$ ions in both He and N_2 buffer gases. Furthermore, we elucidate the structural basis of the aggregation of the metal-bound oligomers with the aid of DFT and trajectory method calculations. As a proof of concept, we then demonstrate the suitability of the tetraorganylborate species as TWIMS calibrants for phenylcuprate and -argentate complexes. Finally, the comparison of experimental and calculated *CCS*s leads to the first ion mobility spectrometry based structural characterization of reactive organometallic anions.

EXPERIMENTAL AND COMPUTATIONAL SECTION

Materials and Synthesis. Alkali-metal tetraphenylborate salts $MBPh_4$ (1,2-dimethoxyethane adduct for M = Li), $NaBEt_4$ and poly-DL-alanine as well as all chemicals required for the synthesis of $NaBXy_4$, $NaB(bPh)_4$ and organometallic reagents were used as purchased. $NaBXy_4$ and $NaB(bPh)_4$ were synthesized according to literature procedures[78,79] as described in the Supporting Information (Section S1). The preparation of solutions of lithium phenylcuprates and -argentates in tetrahydrofuran (THF) was adapted from Putau et al.[70] (for details, see Section S1). Acetonitrile (HPLC grade) was used as solvent for the preparation of solutions of tetraorganylborate salts throughout. Following Forsythe et al.,[47] the polyalanine calibrant solution was obtained by dissolving the polymer in water (Milli-Q® grade; 0.01 mg mL^{-1}). Although neat $NaBEt_4$ needs to be handled under an inert gas atmosphere (it ignites when exposed to air/moisture), its solutions in acetonitrile were found to be stable over a couple of weeks when stored at ~4 °C and protected from sunlight. The other tetraorganylborate salts (as well as their acetonitrile solutions) did not show any indication of air- or moisture-induced decomposition even after several months of storage.

Drift-Tube Ion Mobility-Mass Spectrometry (DTIM-MS) Experiments and Analysis. DTIM-MS experiments were performed in negative-ion mode on a modified Synapt G2-S HDMS Q-IMS-ToF mass spectrometer located in Berlin (Waters) using a nano-ESI or conventional ESI source (see below). The instrument was equipped with an rf-confining drift cell (length: 250.5 ± 0.5 mm), allowing us to obtain ion mobilities (*K*) directly from first principles by the stepped-field method. The mobilities were converted into ^{DT}CCS values via the Mason-Schamp equation.[44,80] ^{DT}CCS values were determined with He or N_2 as buffer gas at ambient temperature and are denoted $^{DT}CCS_{He}$ and $^{DT}CCS_{N2}$, respectively.

For experiments with tetraorganylborates, ions were generated with a nano-ESI source by applying 0.6 to 0.8 kV voltage to in-house prepared, Pt/Pd-coated borosilicate capillaries, filled with ~5 µL of sample solution. The buffer gas pressure was 1.2 Torr for both He and N_2. Reported ^{DT}CCSs are averages of 2 to 3 independent measurements performed on separate days. Air- and moisture-sensitive phenylcuprate and -argentate complexes were measured using a standard ESI source in a similar manner as described in the next section. The buffer gas pressure was 1.8 Torr for both He and N_2. Reported ^{DT}CCS values are averages of 2 independent measurements. Data processing and analysis were carried out using MassLynx 4.1 (Waters) and Origin 2017 (OriginLab) software packages (for further details, see the Supporting Information, Section S2).

Traveling-Wave Ion Mobility-Mass Spectrometry (TWIM-MS) Experiments and Analysis. TWIM-MS experiments were carried out with a commercial Synapt G2-S HDMS Q-IMS-ToF instrument located in Göttingen (Waters) equipped with an ESI source and operated with N_2 as buffer gas. Organometallic and calibrant solutions were injected into the mass spectrometer using a gas-tight syringe at flow rates in the range of 8–33 µL min^{-1}. Before the measurements of the phenylcuprates and –argentates, the source ion block was kept at 150 °C for several hours and the source was flushed with dry THF (~10 mL) to remove traces of air and moisture. Negative-ion mode ESI mass spectra and ATDs for

each organometallic sample were recorded for six different traveling-wave velocities (40 V wave height) well-suited for subsequent measurements of the following calibrant solutions at identical TWIMS settings: $NaBPh_4/CsBPh_4$ (25/25 μM), $NaBXy_4/CsBPh_4$ (25/50 μM), $NaB(bPh)_4/CsBPh_4$ (25/50 μM), $NaBEt_4/CsBPh_4$ (500/50 μM) and polyalanine. For each calibrant solution, mass spectra and ATDs were recorded for three different wave velocities. All TWIM-MS measurements were performed in duplicate (for further details, see the Supporting Information, Section S3).

The software DriftScope 2.7 (Waters) was used for determining the main m/z peak apices of each relevant species of the mass spectra and those of the corresponding ATDs as well as for deriving the ${}^{TW}CCS_{N2}$ values of phenylcuprate and -argentate ions in the following way: The experimental arrival times, t_a, were corrected according to

$$t_a' = t_a - 10^{-3} \cdot c\sqrt{\frac{m}{z}}\,, \qquad (1)$$

where c is the enhanced duty cycle delay coefficient of the instrument.[36] For each calibration measurement, the parameters A and B were determined by fitting the power law

$$\frac{{}^{DT}CCS_{N2}\sqrt{\mu}}{|z|} = {}^{DT}CCS_{N2}' = A \cdot (t_a')^B \qquad (2)$$

to the ${}^{DT}CCS_{N2}'$ vs t_a' data of the calibrant ions, where ${}^{DT}CCS_{N2}'$ is the normalized ${}^{DT}CCS_{N2}$ (values of polyalanine anions taken from Allen et al.[81]).[37] The wave velocity-specific sets of A and B parameters were used to convert the corresponding t_a' values of phenylcuprate and -argentate ions to ${}^{TW}CCS_{N2}$ values on the basis of eq. 2. The given ${}^{TW}CCS_{N2}$ values are the averages of the results obtained for the different traveling-wave velocities.

DFT Calculations. The PBE0 hybrid functional[82] was applied for geometry optimizations, harmonic vibrational frequency calculations and the determination of partial atomic charges, which were all carried out with the Gaussian 09 program package[83,84] (Gaussian 09 settings: SCF=Tight, Int=Fine, Opt=Tight). Molecular structures were optimized using the D3BJ dispersion correction[85,86] as well as def2-SVP basis sets[87] for main group elements and quasi-relativistic effective core potentials[87-89] for copper and silver (ECP10MWB and def2-ECP28MWB, respectively) together with the corresponding valence basis sets.[87-89] Moreover, a PBE0/def2-SVP/ECPMWB re-optimization was conducted for each of the copper- or silver-containing PBE0-D3BJ/def2-SVP/ECPMWB geometries. For every optimized structure, the corresponding DFT electron density was used for computing partial atomic charges by natural population analysis (NPA)[90] and according to the Merz-Singh-Kollman (MK)[91] scheme. In cases where two isomers were identified for a species, their relative Gibbs energy at $T = 298.15$ K, ΔG_{298}, was determined for each of the applied quantum chemical methods. The G_{298} value for an individual structure was obtained by adding together the electronic energy, the zero-point vibrational energy and the thermochemical correction, which was calculated by the quasi-RRHO approach (for further details, see the Supporting Information, Section S4).[92]

Theoretical *CCS* Calculations. Theoretical CCS_{He} and CCS_{N2} values were computed for the DFT-optimized structures. For collisions with He, *CCS*s were determined with the projection approximation (PA) method,[93] the exact hard sphere scattering (EHSS) method[94] and the trajectory method (TM)[95] using a customized version of the original MOBCAL program ($MOBCAL_{He}$), whereas CCS_{N2} values were calculated with the TM by means of adapted variants of the modified MOBCAL version of Kim et al.[96] ($MOBCAL_{N2}$). The TM calculations were carried out for $T = 298$ K for both NPA and MK partial atomic charge distributions (for further details, see the Supporting Information, Section S5, Table S1). For species, for which two energetically closely lying conformers had been identified, the given theoretical *CCS* value corresponds to the Boltzmann-weighted average of their individual *CCS* values.

RESULTS AND DISCUSSION

DTIM-MS Measurements of Tetraorganylborate Monomers and Homo-Oligomers. Upon ESI of acetonitrile solutions of sodium tetraorganylborate salts ($NaBR_4$ with $BR_4^- = BPh_4^-$, BEt_4^-, BXy_4^- and $B(bPh)_4^-$; Scheme 1) in the negative ion mode, not only BR_4^- ions could be generated, but also the spontaneous formation of singly-charged aggregates with the general formula $[Na_{n-1}(BR_4)_n]^-$ occurred (n is referred to as aggregation number).[97] Herein, aggregates are termed homo-oligomers if they contain solely one of the four tetraorganylborate monomers. Aggregates with different BR_4^- units are called hetero-oligomers and will be discussed further below.

First, ion mobilities of the four tetraorganylborate monomers and those of the corresponding Na^+-bound homo-oligomers were measured in He using DTIM-MS, and then converted into ${}^{DT}CCS_{He}$ values (Table S2). Although ${}^{DT}CCS_{He}$ values do not purely reflect molecular surfaces, they are strongly related to the ions' molecular frameworks. Thus, they carry important information about the size and shape of tetraorganylborate aggregates. ATDs of tetraorganylborate monomers and homo-oligomers could be successfully fit with single Gaussians, indicating well-defined gas-phase structures and the lack of multiple structurally different and non-interconverting isomers for a single species (Figure 1a). The linear increase of the ${}^{DT}CCS_{He}$ values of the $[Na_{n-1}(BR_4)_n]^-$ species with increasing n suggests that highly ordered oligomers are formed, displaying linear growth (Figure 1b). Each additional $[Na(BR_4)]$ unit increases the growing aggregate's surface area equally, which is in strong contrast to the isotropic growth of spherical oligomers.[98] In the isotropic growth model, *CCS*s increase in direct proportion to $m^{2/3}$, m being the mass of the oligomers.[99,100] Following the measurements of the $[Na_{n-1}(BR_4)_n]^-$ aggregates, analogous DTIM-MS experiments were carried out on tetraphenylborate homo-oligomers formed with the alkali metal ions Li^+, K^+, Rb^+ and Cs^+. Except for $[Li_{n-1}(BPh_4)_n]^-$, where no oligomers with $n > 2$ were detected, similar linear growth trends were observed for every system, irrespective of the nature of the cation (Table S2). The absence of higher oligomers in the case of lithium most likely is the consequence of a lower binding energy between the hard Lewis acid Li^+ and the soft Lewis base BPh_4^-.[101] In addition, the ${}^{DT}CCS_{He}$ values of corresponding homo-oligomers increased as a function of the van der Waals radii of the metal centers,[102] e.g. for $n = 2$, the smallest and largest *CCS*s belong to $[Li(BPh_4)_2]^-$ and $[Cs(BPh_4)_2]^-$, respectively.

Altogether, ${}^{DT}CCS_{He}$ values of 37 monoanionic tetraorganylborate species were determined, ranging from 81 to 585 Å^2

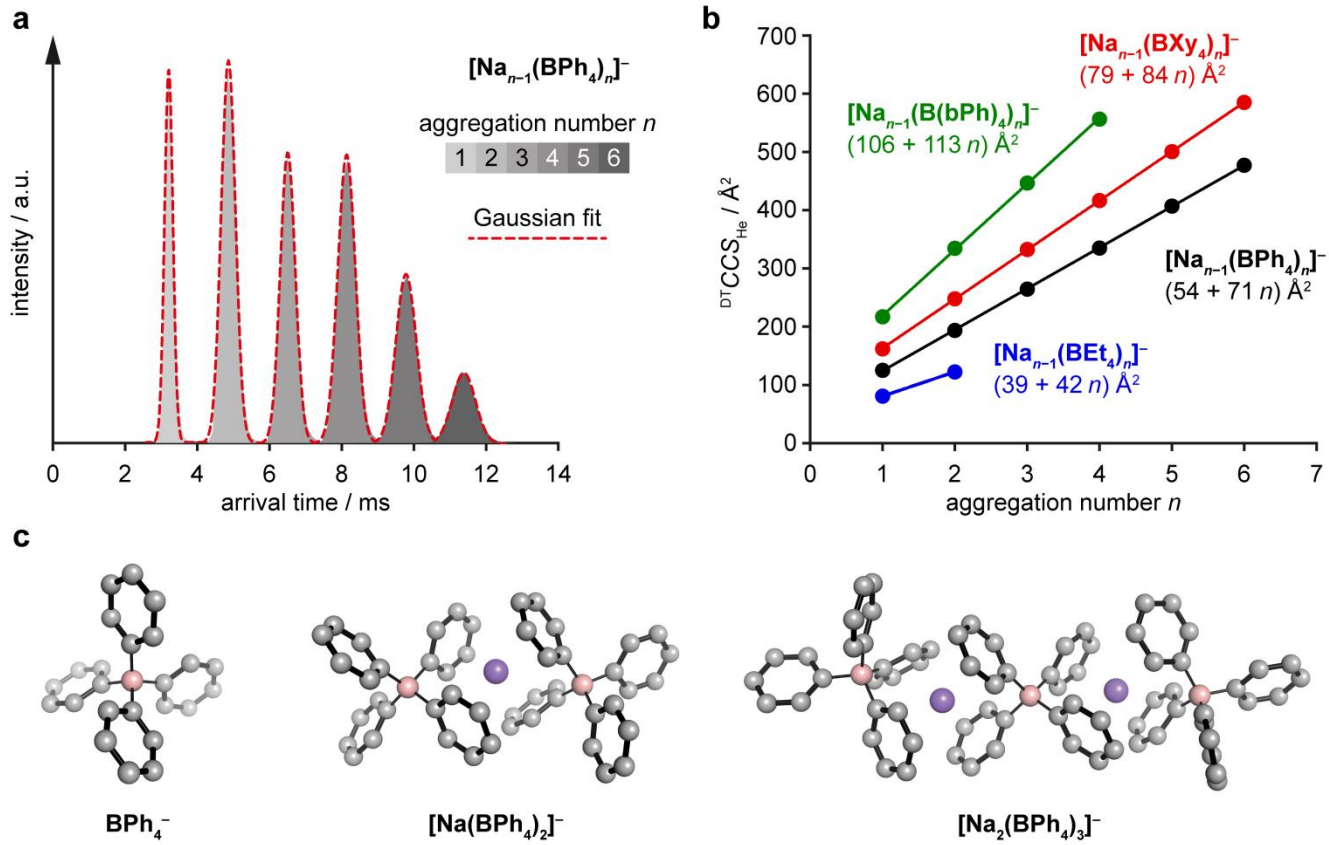

Figure 1. Gas-phase structures and aggregation properties of tetraorganylborate species probed by DTIM-MS and DFT calculations. (a) Superimposed arrival time distributions (ATDs) of $[Na_{n-1}(BPh_4)_n]^-$ species obtained by DTIM-MS in 1.2 Torr He buffer gas at 75 V drift voltage. The more intense signal of the monomer was normalized to the peak of the dimer to facilitate graphical representation. ATDs are unimodal and highly symmetric, resembling Gaussian distributions (red dashed lines). (b) $^{DT}CCS_{He}$ of tetraorganylborate monomers and homo-oligomers formed with Na^+ (circles), depicted as a function of aggregation number n. Linear growth trends are apparent; slopes of the linear functions (lines, color-coded equations shown in the figure) reflect the increase in the molecular surface upon the addition of $[Na(BR_4)]$ units. R^2 of the best-fit lines are 0.99996 for $[Na_{n-1}(BPh_4)_n]^-$ (black), 0.99998 for $[Na_{n-1}(BXy_4)_n]^-$ (red) and 0.99986 for $[Na_{n-1}(B(bPh)_4)_n]^-$ (green). (c) Gas-phase structures of $[Na_{n-1}(BPh_4)_n]^-$ species (n = 1–3) obtained from PBE0-D3BJ/def2-SVP calculations (H atoms omitted for clarity) and verified by comparing their theoretical *CCS*s to those determined experimentally. The DFT calculations reveal the structural basis of the observed growth trend: alternating Na^+ and BPh_4^- ions – held together by cation–π interactions – form linear chains expanding along one dimension, making the accessible surface area proportional to n.

(Figure S1), which already highlights the potential of MBR_4 salts for calibrating TWIMS data. In the context of the latter, N_2 buffer gas plays a prominent role and therefore, we performed analogous DTIM-MS experiments on tetraorganylborate monomers and homo-oligomers in N_2. Essentially the same species were characterized in both buffer gases (for $^{DT}CCS_{N2}$ values, see Table S3) and the above-mentioned linear growth trends were reproduced in N_2 (Figure S2). The uncertainties of the ^{DT}CCSs are estimated to be below 2%.

Calculated Structures and Theoretical *CCS* Values of Tetraorganylborate Species. The calculated PBE0-D3BJ/def2-SVP structures of $[Na_{n-1}(BPh_4)_n]^-$ (n = 1–3) directly reflect the experimentally observed linear growth trends for the $[M_{n-1}(BR_4)_n]^-$ species and thereby suggest that the gaseous tetraorganylborate homo-oligomers correspond to linear chains consisting of alternating M^+ and BR_4^- units (Figure 1c). According to the calculations, these units are bound to each other by specific cation–π interactions in the case of $[Na(BPh_4)_2]^-$ and $[Na_2(BPh_4)_3]^-$, which results in a well-defined coordination environment of the metal centers, i.e., two phenyl rings of one borate together with two phenyl rings of a second borate form one coordination pocket. This structural motif has also been identified in the solid state of alkali metal tetraphenylborate salts by X-ray diffraction.[103] Most likely, it is generally present in tetraorganylborate oligomers with aromatic R groups, which rationalizes that these complexes do not feature multiple isomers as implied by their ATDs.

Given the well-known good performance of the applied geometry-optimization method[104] and the qualitative agreement of the calculated structures of $[Na_{n-1}(BPh_4)_n]^-$ (n = 1–3) with the experimental results, we assume these structures to be quite accurate. Therefore, we also expect the theoretical ^{TM}CCSs to reproduce the measured ^{DT}CCSs in a quantitative manner, provided the former are determined with an appropriately parametrized trajectory method.[105-109] Using MOBCAL$_{He}$ with Lennard-Jones parameters from Campuzano et al. that were optimized for cationic compounds,[106] deviations below 0.4% were obtained between the $^{DT}CCS_{He}$ and $^{TM\text{-}NPA}CCS_{He}$ values for $[Na(BPh_4)_2]^-$ and $[Na_2(BPh_4)_3]^-$ as well as for BXy_4^- and $B(bPh)_4^-$ (Table 1; for the calculated structures of the monomers, see Figure S3). This finding suggests that the calculated geometries are indeed consistent with the actual gas-phase

structures of these species. However, even though the DFT structure for the smaller BPh_4^- monomer is certainly not more error-prone than the others, its $^{TM\text{-}NPA}CCS_{He}$ value is significantly lower than the experimental reference (−4.0%) and for BEt_4^- as the smallest considered borate, the deviation is even more pronounced (−14.0%; Table 1; for the calculated isomers of BEt_4^- and their relative energies, see Figure S3, Table S4). Consequently, the accuracy of the used TM apparently decreases below a certain system size. In line with this trend, Lee et al. have reported similar non-uniform size-dependent deviations between $^{DT}CCS_{He}$ and $^{TM}CCS_{He}$ values for cationic species,[107] which together with our results indicates that the state-of-the-art TM approach does not treat the interactions between molecular ions and buffer gases in an universally correct manner. Nevertheless, there is no indication that the excellent agreement between the $^{DT}CCS_{He}$ and $^{TM\text{-}NPA}CCS_{He}$ values for the larger tetrarylborate species results from error compensation. Thus, the applied TM appears well-suited for providing reliable theoretical CCS_{He} values for sufficiently large organometallic anions (approx. $^{DT}CCS_{He} > 160$ Å^2). In addition, $^{TM\text{-}MK}CCS_{He}$ values were determined for the calculated tetraorganylborate structures as well and were found to be minimally smaller than their $^{TM\text{-}NPA}CCS_{He}$ analogues (Table S5, Figure S4; $^{PA}CCS_{He}$ and $^{EHSS}CCS_{He}$ values are given for completeness).

In contrast to the results for He buffer gas, $^{TM}CCS_{N2}$ values obtained by MOBCAL$_{N2}$ calculations employing optimized force field parameters from Campuzano et al.[106] (denoted as D_i' and x_i' herein) are much larger than the $^{DT}CCS_{N2}$ values for BXy_4^-, $B(bPh)_4^-$ and $[Na_{n-1}(BPh_4)_n]^-$ ($n = 2, 3$), which is more pronounced for NPA charges (Table S6, Figure S5). This difference suggests that the used force field parameters overestimate the attractive van der Waals interaction between N_2 and the investigated anions. As the latter is largely dominated by the C−N pair potentials, we determined scaling factors, $s_{C,NPA}$ and $s_{C,MK}$, for the D_C' parameter that minimize the deviation of the $^{TM\text{-}NPA}CCS_{N2}$ and $^{TM\text{-}MK}CCS_{N2}$ values for the PBE0-D3BJ/def2-SVP structure of $[Na(BPh_4)_2]^-$ from the experimental reference.[110] $[Na(BPh_4)_2]^-$ was chosen for the optimization procedure, because this ion is supposedly more rigid than BXy_4^-, $B(bPh)_4^-$ and $[Na_2(BPh_4)_3]^-$. For NPA and MK charges, $s_{C,NPA} = 0.28$ and $s_{C,MK} = 0.52$ were ascertained as optimal scaling factors, respectively. By means of these factors, nearly the same agreement was achieved between the $^{DT}CCS_{N2}$ and $^{TM}CCS_{N2}$ values for the tetraorganylborate species as in the case of He (Tables 1 and S6, Figure S5).[111] The mean absolute relative deviation (*MARD*) of the final $^{TM\text{-}MK}CCS_{N2}$ values is minimally smaller than for their $^{TM\text{-}NPA}CCS_{N2}$ counterparts. Furthermore, the deviations of the $^{TM}CCS_{N2}$ values for BEt_4^- are not as pronounced as for the corresponding $^{TM}CCS_{He}$ values, but also upon application of the re-optimized TM for N_2 buffer gas, reliable theoretical *CCS*s can only be expected for larger organometallic anions (approx. $^{DT}CCS_{N2} > 220$ Å^2).

Full Set of ^{DT}CCS values of Tetraorganylborate Species. To extend the set of tetraorganylborate species that can be used for TWIMS calibration, we performed ESI-DTIM-MS measurements of acetonitrile solutions containing $NaBR_4$ ($BR_4^- = BPh_4^-$, BEt_4^-, BXy_4^- and $B(bPh)_4^-$) and $CsBPh_4$ with N_2 buffer gas.[112] Owing to their spontaneous aggregation during the ESI process, this small set of tetraorganylborate salts allowed us to measure $^{DT}CCS_{N2}$ values of a large number of sodium- and cesium-bound hetero-oligomers (42) as well as additional Cs-bound homo-oligomers (Table S3; heterometallic species were not considered). In total, 76 $^{DT}CCS_{N2}$ values of tetraorganylborate species were determined, ranging from 130 to 704 Å^2 (Figure 2a). As all $^{DT}CCS_{N2}$ values correspond to singly-charged ions, they cover not only a broad range of *CCS*s, but also remarkably wide ranges of normalized *CCS*s and mobilities, which substantially exceed those of the available polyalanine calibrant monoanions.[81]

Figure 2b illustrates a selection of possibilities arising from the modularity of the tetraorganylborate-alkali metal system. The four two-component mixtures presented ($NaBPh_4/CsBPh_4$, $NaBEt_4/CsBPh_4$, $NaBXy_4/CsBPh_4$, $NaB(bPh)_4/CsBPh_4$) offer the coverage of different ranges of $^{DT}CCS_{N2}$ values and also differ with respect to the number of calibrant ions attainable through their application (for the corresponding calibration tables, see Tables S7–S10). On the basis of the full set of $^{DT}CCS_{N2}$ values of tetraorganylborate species determined in this study, we consider these four mixtures as particularly useful for the calibration of TWIMS measurements of a variety of samples and therefore tested their performance in detail (see next section). However, they are only representative examples. The flexibility of the $[M_{n-1}(BR_4)_n]^-$ systems allows analysts to tailor calibrant mixtures to their own needs. Moreover, the pool of calibrant ions may be readily extended in the future by implementing further BAr_4^- building blocks that are compatible with the current set of species.

Application of Tetraorganylborate Calibrants to TWIM-MS Measurements of Phenylcuprates and -argentates. ESI-TWIM-MS experiments on solutions of the prototypical organocuprate $LiCuPh_2$·LiI in THF yielded mass spectra similar to those previously recorded by ESI-quadrupole ion trap MS:[70] the monomeric $[CuPh_2]^-$ complex and the lithium-bound trimer $[Li_2Cu_3Ph_6]^-$

Table 1. Comparison Between Experimental ^{DT}CCS and Theoretical ^{TM}CCS Values[a] of Tetraorganylborate Species.

	$^{DT}CCS_{He}$ / Å^2	$^{TM\text{-}NPA}CCS_{He}$ / Å^2	$\Delta_{\%}$[b] / %	$^{DT}CCS_{N2}$ / Å^2	$^{TM\text{-}MK}CCS_{N2}$[c] / Å^2	$\Delta_{\%}$[b] / %
BPh_4^-	125.3	120.3	−4.0	185.2	177.7	−4.0
$[Na(BPh_4)_2]^-$	193.9	194.1	0.1	265.6	265.3	−0.1
$[Na_2(BPh_4)_3]^-$	264.5	264.4	0.0	350.7	347.9	−0.8
BEt_4^-[d]	80.7	69.4	−14.0	130.3	118.5	−9.0
BXy_4^-	162.0	161.6	−0.3	224.0	224.3	0.2
$B(bPh)_4^-$	216.9	216.2	−0.3	294.4	298.3	1.3

[a]Applied structures and partial charges obtained from PBE0-D3BJ/def2-SVP calculations. [b]Deviation of ^{TM}CCS from ^{DT}CCS relative to the latter in percent. [c]Trajectory method has been optimized to reproduce the $^{DT}CCS_{N2}$ value of $[Na(BPh_4)_2]^-$; the scaling factor applied to the D_C' parameter was optimized with a precision of 0.01. [d]Theoretical *CCS* values are Boltzmann-weighted averages over two conformers.

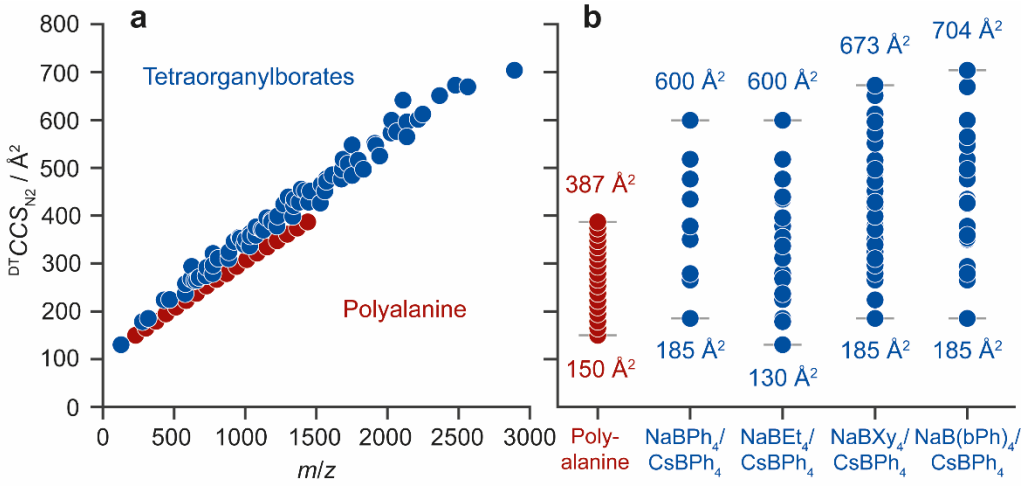

Figure 2. Collision cross sections of anionic tetraorganylborate species in N_2 buffer gas – establishing a modular set of calibrants for ion mobility spectrometry. (a) A total of 76 $^{DT}CCS_{N2}$ values were determined, spanning a range of 130–704 Å² (blue circles). All 76 singly-charged ions were generated using four tetraorganylborate anions (BPh_4^-, BEt_4^-, BXy_4^-, $B(bPh)_4^-$) together with alkali metal cations (Li^+, Na^+, K^+, Rb^+, Cs^+). Singly-charged ions from poly-DL-alanine ($[Ala_n - H]^-$, $n = 3–20$) – a common collision cross section calibrant for negative ions – are plotted in red for comparison (values adopted from Allen et al.,[81] representing an extended set in comparison to previous studies[47]). (b) $^{DT}CCS_{N2}$ of calibrant ions accessible by employing polyalanine (red) or simple two-component mixtures of tetraorganylborate salts (blue). Minima and maxima of the respective collision cross section ranges are highlighted. The number of ions attainable using the different calibrants are: 18 (polyalanine), 9 ($NaBPh_4/CsBPh_4$), 19 ($NaBEt_4/CsBPh_4$), 30 ($NaBXy_4/CsBPh_4$) and 21 ($NaB(bPh)_4/CsBPh_4$).

were obtained as the main species and the oligomeric complexes $[Cu_nPh_{n+1}]^-$ ($n = 2, 3$) and $[LiCu_2Ph_4]^-$ were observed as well (Figure 3a). This finding demonstrates that IM-MS, just as conventional MS, is an appropriate tool for the investigation of sensitive organometallic reagents. In addition, TWIM-MS measurements of solutions of $LiAgPh_2$·LiI in THF were also carried out and analogous species were detected as in the case of the lithium phenylcuprate samples, which shows the similarity of the two coinage metallate solutions (Figure S6). For all of the observed phenylcuprate and -argentate ions, unimodal ATDs were measured, indicating that these are structurally well-defined species (Figure S6).

In order to obtain $^{TW}CCS_{N2}$ values for the cuprate and -argentate complexes, *CCS* calibration curves according to eq. 2 were determined on the basis of TWIMS calibration measurements using the aforementioned two-component tetraorganylborate salt mixtures as well as polyalanine (for representative mass spectra of the former, see Figure S7). For the generation of the calibration curves based on the $NaBPh_4/CsBPh_4$, $NaBEt_4/CsBPh_4$, $NaBXy_4/CsBPh_4$, $NaB(bPh)_4/CsBPh_4$ and polyalanine calibrants, 5, 12, 11, 8 and 15 calibrant ions were considered, respectively, spanning similar $^{DT}CCS_{N2}$ ranges (Tables S7–S10). In all cases, the average R^2 value of the power-law fits for the $^{DT}CCS_{N2}$' vs t_a' data was at least 0.9998 (for representative calibration curves, see Figures 3b and S8; for *A* and *B* values of all calibration measurements, see Table S11), which highlights the internal consistency of the $^{DT}CCS_{N2}$ values of the tetraorganylborate ions. The average $^{TW}CCS_{N2}$ values derived for the phenylcuprate and -argentate species have relative standard deviations below 0.2% on average for all considered calibrants (Table S12) and are discussed in comparison with the corresponding $^{DT}CCS_{N2}$ values in the following section.

DTIM-MS Measurements of Phenylcuprates and -argentates and Comparison with TWIM-MS Results. Solutions of $LiMPh_2$·LiI (M = Cu, Ag) in THF were also investigated by ESI-DTIM-MS. In doing so, ion mobilities and ^{DT}CCSs of all phenylcuprate and -argentates ions detected by the TWIM-MS measurements could be determined in both He and N_2 (Tables S13 and S14). Furthermore, additional coinage-metal complexes were observed and characterized within the DTIM-MS experiments, viz. $[M_nPh_{n+1}]^-$ ($n = 4, 5$) and $[LiM_4Ph_6]^-$ as well as $[Cu_8Ph_9]^-$ and $[Ag_nPh_{n+1}]^-$ ($n = 6, 7$). This manifold of detected species highlights once more the well-known complexity of speciation of organometallic reagents in solution.[1-6] As the ^{DT}CCS values are obtained from first principles, they are ideal for benchmarking the corresponding $^{TW}CCS_{N2}$ values and thus, to assess the suitability of the established polyalanine and the here-introduced tetraorganylborate *CCS* calibrants for TWIM-MS measurements of organometallic anions. Moreover, the ^{DT}CCS values serve as reference points for the comparison with theoretical *CCS*s to elucidate the structures of selected phenylcuprates and -argentates.

Independent of the applied tetraorganylborate calibrant mixture, all determined $^{TW}CCS_{N2}$ values for the coinage metallate species deviate less than 2% from their $^{DT}CCS_{N2}$ counterparts (Figures 3c and S9, Table S15),[113,114] although the $[M_nPh_{n+1}]^-$ complexes ($n = 1, 2$) feature $^{DT}CCS_{N2}$ values, which are slightly below the *CCS* range of the $NaBPh_4/CsBPh_4$, $NaBXy_4/CsBPh_4$ and $NaB(bPh)_4/CsBPh_4$ calibrants. In many cases, the deviation is even below 1% and hence, well within the estimated experimental uncertainty of the $^{DT}CCS_{N2}$ values. In this regard, the *MARD*s associated with the $NaBEt_4/CsBPh_4$ and $NaBXy_4/CsBPh_4$ calibrants are remarkable in particular (0.7 and 0.5%, respectively), which might result from the fact that these mixtures cover the *CCS* space in a

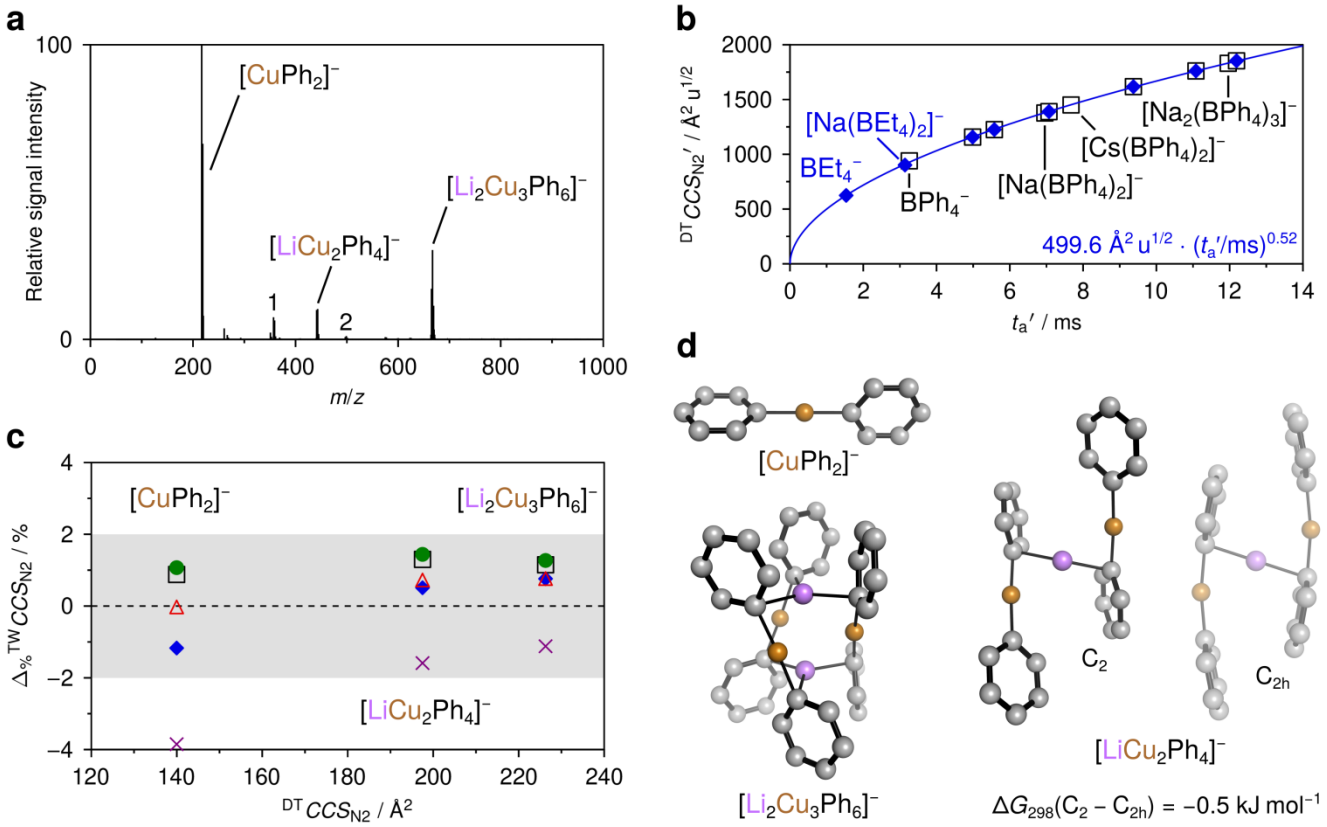

Figure 3. Ion mobility-mass spectrometry and DFT calculations for the structural characterization of gaseous phenylcuprate ions. (a) Negative-ion mode ESI mass spectrum of a ~25 mM solution of $LiCuPh_2$·LiI in THF recorded with a commercial Synapt G2-S HDMS instrument (TWIM-MS). 1: $[Cu_2Ph_3]^-$, 2: $[Cu_3Ph_4]^-$. (b) $^{DT}CCS_{N2}'$ vs. t_a' data set for the TWIMS calibration measurement (traveling-wave velocity of 1050 m s^{-1}) of a solution of $NaBEt_4$/$CsBPh_4$ (500/50 µM) in acetonitrile (symbols) as well as the corresponding power-law fit according to eq. 2 (line, equation shown in the figure, $R^2 = 0.9999$). Data points of tetraorganylborate hetero-oligomers are unlabeled and represented by two superimposed symbols. (c) Relative deviations of $^{TW}CCS_{N2}$ values of phenylcuprate species determined with the help of TWIMS calibration measurements of solutions of $NaBPh_4$/$CsBPh_4$ (open black squares), $NaBEt_4$/$CsBPh_4$ (full blue diamonds), $NaBXy_4$/$CsBPh_4$ (open red triangles), $NaB(bPh)_4$/$CsBPh_4$ (full green circles) and polyalanine (purple crosses) from $^{DT}CCS_{N2}$ values plotted against the latter. The gray area indicates the deviation range that is typically achieved for $^{TW}CCS_{N2}$ values in the case of matched analyte and calibrant ions. (d) Gas-phase structures of phenylcuprate species obtained from PBE0-D3BJ/def2-SVP/ECP10MWB calculations (H atoms are omitted for clarity). The calculated geometries of $[CuPh_2]^-$ and $[Li_2Cu_3Ph_6]^-$ could be verified by comparing their theoretical *CCS*s to those determined experimentally. In the case of $[LiCu_2Ph_4]^-$, the comparison suggests that the C_{2h}-symmetric conformer is less populated than predicted by the DFT calculations.

more balanced manner than the others. Consequently, our benchmark study provides evidence that all considered BR_4^- species and their aggregates formed with alkali metal cations are ideal calibrant ions for the determination of accurate $^{TW}CCS_{N2}$ values of organometallic anions. In comparison with the tetraorganylborate calibrants, the application of polyalanine yields systematically smaller $^{TW}CCS_{N2}$ values for the coinage metallates (Figures 3c and S9, Table S15). However, their overall agreement with respect to the reference values is quite good (*MARD* of 2.0%) and only for the $[MPh_2]^-$ species, they show deviations significantly larger than 2%.

Apart from their value for testing the applicability of the different TWIMS calibrants, the obtained ^{DT}CCSs for the coinage metal complexes also afford information on the structures of the latter. Pairs of matching phenylcuprate and -argentate species exhibit strikingly similar ^{DT}CCS values (Tables S13 and S14), which suggests that they have analogous structures. Accordingly, identical growth trends for $[M_nPh_{n+1}]^-$ as well as for $[Li_{n-1}M_nPh_{2n}]^-$ ions as function of n could be ascertained irrespective of the coinage metal M (Figure S10). While an approximately linear growth holds for the $[M_nPh_{n+1}]^-$ species for n = 1–4, the addition of another [MPh] unit to $[M_4Ph_5]^-$ leads to pentanuclear complexes with a more compact structure compared to the lower oligomers.[115] Likewise, the pentanuclear $[Li_2M_3Ph_6]^-$ ions are denser than the corresponding lithium-bound dimers $[LiM_2Ph_4]^-$. Thus, ESI-IMS affords intimate insight into the structures of organometallate complexes.

Calculated Structures and Theoretical *CCS* Values of Phenylcuprates and -argentates. For each type of the theoretically investigated coinage metallate complexes, viz. $[M_nPh_{n+1}]^-$ (n = 1–3, 5) and $[Li_{n-1}M_nPh_{2n}]^-$ (n = 2, 3), analogous structures were identified by PBE0-D3BJ/def2-SVP/ECPMWB calculations for M = Cu and Ag (Figures 3d and S11) in accordance with their ^{DT}CCS values. In the cases of $[M_3Ph_4]^-$ and $[LiM_2Ph_4]^-$, this equivalence includes two conformers, respectively, which are both substantially populated based on their Gibbs energy difference (Table S16). The calculated geometries indicate that the $[MPh_2]^-$ species are linear complexes in agreement with the crystal structure[116] found for $[CuPh_2]^-$ and a previous gas-phase study[117] on $[AgPh_2]^-$. Furthermore, the larger $[M_nPh_{n+1}]^-$ aggregates can be considered as chains

Table 2. Comparison Between Experimental ^{DT}CCS and Theoretical ^{TM}CCS Values[a] of Phenylcuprates and -argentates.

		$^{DT}CCS_{He}$ / Å^2	$^{TM\text{-}NPA}CCS_{He}$ / Å^2	$\Delta_{\%}$[b] / %	$^{DT}CCS_{N2}$ / Å^2	$^{TM\text{-}MK}CCS_{N2}$[c] / Å^2	$\Delta_{\%}$[b] / %
$[CuPh_2]^-$		88.3	82.4	−6.6	140.0	135.1	−3.5
$[LiCu_2Ph_4]^-$ [d,e]		138.9	130.8	−5.9	197.5	185.0	−6.3
	C_2		134.8	−2.9		189.3	−4.1
	C_{2h}		125.8	−9.4		179.8	−9.0
$[Li_2Cu_3Ph_6]^-$		161.4	157.8	−2.2	226.3	212.2	−6.2
$[AgPh_2]^-$		88.8	83.6	−5.9	141.8	138.3	−2.5
$[LiAg_2Ph_4]^-$ [d,e]		140.6	134.9	−4.1	202.5	190.3	−6.0
	C_2		139.0	−1.1		194.3	−4.1
	C_{2h}		129.1	−8.2		184.7	−8.8
$[Li_2Ag_3Ph_6]^-$		163.2	160.0	−2.0	229.5	215.1	−6.3

[a]Applied structures and partial charges obtained from PBE0-D3BJ/def2-SVP/ECPMWB calculations. [b]Deviation of ^{TM}CCS from ^{DT}CCS relative to the latter. [c]Trajectory method has been optimized to reproduce the $^{DT}CCS_{N2}$ value of $[Na(BPh_4)_2]^-$. [d]Theoretical *CCS* values are Boltzmann-weighted averages over two conformers. [e]Theoretical *CCS* values of the individual conformers (C_2 and C_{2h}) are also given.

consisting of alternating Ph^- and M^+ units for $n = 2$ and 3, whereas $n = 5$ involves a more compact arrangement, where the metal centers form a trigonal bipyramid and all phenyl groups correspond to μ_2-bridging ligands. Exactly this kind of structure is known for the pentanuclear $[Cu_5Ph_6]^-$, $[Li_2Cu_3Ph_6]^-$ and $[Li_2Ag_3Ph_6]^-$ ions in the solid state[118-120] and was also obtained for the latter two by our DFT calculations. Similarly, the determined gas-phase geometries for the $[LiM_2Ph_4]^-$ species are comparable to their homonuclear congeners as well. Thus, the calculated structures for the phenylcuprate and -argentate species are consistent with the experimentally observed growth trends detailed above.

The comparison between the theoretical $^{TM\text{-}NPA}CCS_{He}$ values for the $[M_nPh_{n+1}]^-$ complexes ($n = 1$–3) and the corresponding $^{DT}CCS_{He}$ values further confirms the validity of the DFT structures identified for these ions. While the agreement is excellent for $n = 3$, the deviations increase with decreasing system size (−6.6/−5.9% for $n = 1$ for M = Cu/Ag; Tables 2 and S17, Figure S12) as expected for the TM calculations on the basis of the results for the tetraorganylborates. In contrast to this trend, the $^{TM\text{-}NPA}CCS_{He}$ values for the $[M_5Ph_6]^-$ species are noticeably smaller than the experimental reference (−3.3/−3.2% for M = Cu/Ag), which also holds true for the $[LiM_2Ph_4]^-$ and $[Li_2M_3Ph_6]^-$complexes (Tables 2 and S17, Figure S12; $^{PA}CCS_{He}$ and $^{EHSS}CCS_{He}$ values are given for completeness). Although these discrepancies are not large enough to point to qualitatively wrong candidate structures, they suggest that the DFT calculations predict too compact geometries for the pentanuclear ions as well as a too high population of the C_{2h}-symmetric $[LiM_2Ph_4]^-$ conformers, which feature significantly lower $^{TM\text{-}NPA}CCS_{He}$ values than the corresponding C_2-symmetric structures. Interestingly, using PBE0/def2-SVP/ECPMWB geometries for the phenylcuprates and -argentates (Figure S13, Table S18) instead of the dispersion-corrected analogues causes the largest increase of the $^{TM\text{-}NPA}CCS_{He}$ values for the pentanuclear ions and the lithium-bound dimers (Table S19, Figure S12; $^{PA}CCS_{He}$ and $^{EHSS}CCS_{He}$ values are given for completeness). For the latter, this effect mainly arises from the fact that the more compact C_{2h}-symmetric conformers are not stable without the consideration of dispersion interaction. Consequently, our findings may possibly indicate that the PBE0-D3BJ/def2-SVP/ECPMWB approach overestimates the dispersion interaction between neighboring phenyl ligands. As with the tetraorganylborate species, $^{TM\text{-}MK}CCS_{He}$ values are very similar to the $^{TM\text{-}NPA}CCS_{He}$ values for the coinage metallate complexes (Tables S17 and S19, Figure S14).

Contrary to the results for the tetraorganylborates, the $^{TM}CCS_{N2}$ values for the phenylcuprate and -argentate species determined with the optimized TM approach show deviations from the corresponding $^{DT}CCS_{N2}$ values that significantly differ from those obtained for He buffer gas in most of the cases (Tables 2 and S20, Figure S15). In particular, the $^{TM\text{-}NPA}CCS_{N2}$ values appear to be systematically too small, implying that the optimal scaling factor for the D_C' parameter is larger for the coinage metallates than for the borates when NPA charges are applied. For MSK charges, this inconsistency does not seem to hold, given that the agreement between the $^{DT}CCS_{N2}$ and $^{TM\text{-}MK}CCS_{N2}$ values for the $[M_nPh_{n+1}]^-$ complexes ($n = 1$–3) is even slightly better than between their He counterparts. However, for the pentanuclear $[Li_2M_3Ph_6]^-$ and $[M_5Ph_6]^-$ ions, also the $^{TM\text{-}MK}CCS_{N2}$ values deviate much more from the experimental reference than in the case of He. Apparently, the reliability of the employed TM for the computation of $^{TM\text{-}MK}CCS_{N2}$ values cannot compete with that of the $^{TM}CCS_{He}$ calculations for organometallic anions.

CONCLUSION

We have introduced and characterized a new class of *CCS* calibrants for TWIMS measurements of organometallic anions, which are based on easily accessible alkali metal tetraorganylborate salts. Upon ESI of solutions of these salts, not only borate monomers are produced, but also a large number of alkali-metal-bound oligomers form spontaneously in a modular manner. On this basis, starting from only a few building blocks, we were able to determine ^{DT}CCS values in He and N_2 for a large number of monoanionic tetraorganylborate species, spanning a broad range of 81–585 Å^2 and 130–704 Å^2, respectively. The aggregation of the borates is associated with a linear growth, which originates from a well-defined chain-like assembly of alternating borate and metal cation units as indicated by structures from DFT calculations. While the latter were confirmed by the comparison of their theoretical $^{TM}CCS_{He}$ values with the corresponding experimental *CCS*s, the analogous comparison for the results for N_2 buffer gas prompted us to derive an improved Lennard-Jones parametrization for $^{TM}CCS_{N2}$ calculations for the considered compound class. Using the tetraorganylborate calibrant ions for the *CCS* calibration of TWIMS measurements of

prototypical organometallic anions, viz. phenylcuprates and -argentates, $^{TW}CCS_{N2}$ values in excellent agreement with the results from DTIMS experiments were obtained for these species (*MARD* of ~1%), which highlights the utility of the novel calibrants. The experimental *CCS*s of the observed coinage metallate complexes in combination with computational investigations reveal the structural similarity between copper- and silver-containing congeners and moreover, that the pentanuclear species feature the same compact coordination motif in the gas phase as known from the solid state. Thus, we have demonstrated the capability of IMS experiments for the structural characterization of reactive organometallic anions and in particular, the potential of tetraorganylborate compounds for *CCS* calibration. The extension of this approach to the analysis of further classes of organometallics holds great promise.

ASSOCIATED CONTENT

Supporting Information

The Supporting Information is available free of charge on the ACS Publication website at DOI: 10.1021/acs.anal-chemXXXXXXX.

Synthesis of tetraorganylborate salts and organometallic reagents; details of IM-MS experiments and analysis; details of DFT and theoretical *CCS* calculations; ^{DT}CCS values, calculated structures and theoretical *CCS* values of tetraorganylborate species; CCS_{N2} tables for TWIMS calibration using tetraorganylborate salt solutions; results from TWIM-MS measurements of phenylcuprates and –argentates; ^{DT}CCS values, calculates structures and theoretical *CCS* values of phenylcuprates and -argentates (PDF)

XYZ coordinates (in Å) and partial charges of the calculated structures (ZIP)

AUTHOR INFORMATION

Corresponding Authors

*kevin.pagel@fu-berlin.de

*konrad.koszinowski@chemie.uni-goettingen.de

ORCID

Márkó Grabarics: 0000-0002-2550-637X

Maria Schlangen: 0000-0002-8783-6788

Kevin Pagel: 0000-0001-8054-4718

Konrad Koszinowski: 0000-0001-7352-5789

Author Contributions

§T.A. and M.G. contributed equally.

Notes

The authors declare no competing financial interest.

ACKNOWLEDGMENTS

We gratefully acknowledge support from the Deutsche Forschungsgemeinschaft, 389479699/GRK2455 (T.A., K.K.), KO2875/6-2 (T.A., K.K.) and FOR2177/P03 (M.G., K.P.) as well as the Niedersächsisches Ministerium für Wissenschaft und Kultur, INST 186/1132-1 FUGG (T.A., K.K.). We furthermore thank Dr. Marlene Kolter for her help with the synthesis of tetraorganylborate salts.

REFERENCES

(1) Schlenk, W.; Schlenk, W., jun. *Ber. Dtsch. Chem. Ges.* **1929**, *62*, 920-924.

(2) G. Wilkinson, *Angew. Chem.* **1974**, *86*, 664-667.

(3) Ashby, E. C. *Pure Appl. Chem.* **1980**, *52*, 545-569.

(4) Lambert, C.; von R. Schleyer, P. *Angew. Chem. Int. Ed. Engl.* **1994**, *33*, 1129-1140.

(5) Nakamura, E.; Mori, S. *Angew. Chem. Int. Ed.* **2000**, *39*, 3750-3771.

(6) Sherry, B. D.; Fürstner, A. *Acc. Chem. Res.* **2008**, *41*, 1500-1511.

(7) Henderson, W.; McIndoe, J. S. *Mass Spectrometry of Inorganic, Coordination and Organometallic Compounds: Tools, Techniques, Tips*; Wiley: Chichester, 2005; pp 175-219.

(8) Hanratty, M. A.; Beauchamp, J. L.; Illies, A. J.; Van Koppen, P.; Bowers, M. T. *J. Am. Chem. Soc.* **1988**, *110*, 1-14.

(9) Eller, K.; Schwarz, H. *Chem. Rev.* **1991**, *91*, 1121-1177.

(10) Freiser, B. S. *Acc. Chem. Res.* **1994**, *27*, 353-360.

(11) Armentrout, P. B. *Acc. Chem. Res.* **1995**, *28*, 430-436.

(12) O'Hair, R. A. J. *Chem. Commun.* **2006**, 1469-1481.

(13) Roithová, J.; Schröder, D. *Chem. Rev.* **2010**, *110*, 1170-1211.

(14) Mehara, J.; Roithová, R. *Chem. Sci.* **2020**, *11*, 11960-11972.

(15) Yamashita, M.; Fenn, J. B. *J. Phys. Chem.* **1984**, *88*, 4451-4459.

(16) Traeger, J. C. *Int. J. Mass Spectrom.* **2000**, *200*, 387-401.

(17) Plattner, D. A. *Int. J. Mass Spectrom.* **2001**, *207*, 125-144.

(18) Chen, P. *Angew. Chem. Int. Ed.* **2003**, *42*, 2832-2847.

(19) Santos, L. S.; Knaack, L.; Metzger, J. O. *Int. J. Mass Spectrom.* **2005**, *246*, 84-104.

(20) D. Schröder, *Acc. Chem. Res.* **2012**, *45*, 1521-1532.

(21) Vikse, K. L.; Ahmadi, Z.; McIndoe, J. S. Coord. *Chem. Rev.* **2014**, *279*, 96-114.

(22) MacAleese, L.; Maître, P. *Mass Spectrom. Rev.* **2007**, *26*, 583-605.

(23) Roithová, J. *Chem. Soc. Rev.* **2012**, *41*, 547-559.

(24) Jašíková, L.; Roithová, J. *Chem. Eur. J.* **2018**, *24*, 3374-3390.

(25) Schwarz, H.; Asmis, K. R. *Chem. Eur. J.* **2019**, *25*, 2112-2126.

(26) Kanu, A. B.; Dwivedi, P.; Tam, M.; Matz, L.; Hill, H. H. *J. Mass Spectrom.* **2008**, *43*, 1-22.

(27) Lapthorn, C.; Pullen, F.; Chowdhry, B. Z. *Mass Spectrom. Rev.* **2013**, *32*, 43-71.

(28) May, J. C.; McLean, J. A. *Anal. Chem.* **2015**, *87*, 1422-1436.

(29) Dodds, J. N.; Baker, E. S. *J. Am. Soc. Mass Spectrom.* **2019**, *30*, 2185-2195.

(30) Giles, K.; Pringle, S. D.; Worthington, K. R.; Little, D.; Wildgoose, J. L.; Bateman, R. H. *Rapid Commun. Mass Spectrom.* **2004**, *18*, 2401-2414.

(31) Pringle, S. D.; Giles, K.; Wildgoose, J. L.; Williams, J. P.; Slade, S. E.; Thalassinos, K.; Bateman, R. H.; Bowers, M. T.; Scrivens, J. H. *Int. J. Mass Spectrom.* **2007**, *261*, 1-12.

(32) Campuzano, I. D. G.; Giles, K. *TrAC Trends Anal. Chem.* **2019**, *120*, 115620.

(33) Shvartsburg, A. A.; Smith, R. D. *Anal. Chem.* **2008**, *80*, 9689-9699.

(34) Richardson, K.; Langridge, D.; Giles, K. *Int. J. Mass Spectrom.* **2018**, *428*, 71–80.

(35) Here, the superscript indicates the employed method. This designation style is used for all determined *CCS*s.

(36) Ruotolo, B. T.; Benesch, J. L. P.; Sandercock, A. M.; Hyung, S.-J.; Robinson, C. V. *Nat. Protoc.* **2008**, *3*, 1139-1152.

(37) Smith, D. P.; Knapman, T. W.; Campuzano, I.; Malham, R. W.; Berryman, J. T.; Radford, S. E.; Ashcroft, A. E. *Eur. J. Mass Spectrom.* **2009**, *15*, 113-130.

(38) Bush, M. F.; Hall, Z.; Giles, K.; Hoyes, J.; Robinson, C. V.; Ruotolo, B. T. *Anal. Chem.* **2010**, *82*, 9557-9565.

(39) Ridenour, W. B.; Kliman, M.; McLean, J. A.; Caprioli, R. M. *Anal. Chem.* **2010**, *82*, 1881-1889.

(40) Pagel, K.; Harvey, D. J. *Anal. Chem.* **2013**, *85*, 5138-5145.

(41) Gelb, A. S.; Jarratt, R. E.; Huang, Y.; Dodds, E. D. *Anal. Chem.* **2014**, *86*, 11396-11402.

(42) Hines, K. M.; May, J. C.; McLean, J. A.; Xu, L. *Anal. Chem.* **2016**, *88*, 7329-7336.

(43) Gabelica, V.; Marklund, E. *Curr. Opin. Chem. Biol.* **2018**, *42*, 51-59.

(44) Gabelica, V.; Shvartsburg, A. A.; Afonso, C.; Barran, P.; Benesch, J. L. P.; Bleiholder, C.; Bowers, M. T.; Bilbao, A.; Bush, M. F.; Campbell, J. L.; Campuzano, I. D. G.; Causon, T.; Clowers, B. H.; Creaser, C. S.; De Pauw, E.; Far, J.; Fernandez-Lima, F.; Fjeldsted, J. C.; Giles, K.; Groessl, M.; Hogan, C. J., Jr.; Hann, S.; Kim, H. I.; Kurulugama, R. T., May, J. C.; McLean, J. A.; Pagel, K.; Richardson, K.; Ridgeway, M. E.; Rosu, F.; Sobott, F.;Thalassinos, K.; Valentine, S. J.; Wyttenbach, T. *Mass Spectrom. Rev.* **2019**, *38*, 291-320.

(45) Bush, M. F.; Campuzano, I. D. G.; Robinson, C. V. *Anal. Chem.* **2012**, *84*, 7124-7130.

(46) Hofmann, J.; Struwe, W. B.; Scarff, C. A.; Scrivens, J. H.; Harvey, D. J.; Pagel, K. *Anal. Chem.* **2014**, *86*, 10789-10795.

(47) Forsythe, J. G.; Petrov, A. S.; Walker, C. A.; Allen, S. J.; Pellissier, J. S.; Bush, M. F.; Hud, N. V.; Fernández, F. M. *Analyst* **2015**, *140*, 6853-6861.

(48) Duez, Q.; Chirot, F.; Liénard, R.; Josse, T.; Choi, C.; Coulembier, O.; Dugourd, P.; Cornil, J.; Gerbaux, P.; De Winter, J. *J. Am. Soc. Mass Spectrom.* **2017**, *28*, 2483-2491.

(49) Haler, J. R. N.; Kune, C.; Massonnet, P.; Comby-Zerbino, C.; Jordens, J.; Honing, M.; Mengerink, Y.; Far, J.; De Pauw, E. *Anal. Chem.* **2017**, *89*, 12076-12086.

(50) Hupin, S.; Lavanant, H.; Renaudineau, S.; Proust, A.; Izzet, G.; Groessl, M.; Afonso, C. *Rapid Commun. Mass Spectrom.* **2018**, *32*, 1703-1710.

(51) Lavanant, H.; Groessl, M.; Afonso, C. *Int. J. of Mass Spectrom.* **2019**, *442*, 14-22.

(52) May, J. C.; Morris, C. B.; McLean, J. A. *Anal. Chem.* **2017**, *89*, 1032-1044.

(53) Stow, S. M.; Causon, T. J.; Zheng, X.; Kurulugama, R. T.; Mairinger, T.; May, J. C.; Rennie, E. E.; Baker, E. S.; Smith, R. D.; McLean, J. A.; Hann, S.; Fjeldsted, J. C. *Anal. Chem.* **2017**, *89*, 9048-9055.

(54) For TWIMS studies on cationic organometallic compounds, see: Williams, J. P.; Bugarcic, T.; Habtemariam, A.; Giles, K.; Campuzano, I.; Rodger, P. M.; Sadler, P. J. *J. Am. Soc. Mass Spectrom.* **2009**, *20*, 1119-1122, as well as refs 55-58.

(55) Williams, J. P.; Lough, J. A.; Campuzano, I.; Richardson, K.; Sadler, P. J. *Rapid Commun. Mass Spectrom.* **2009**, *23*, 3563-3569.

(56) Czerwinska, I.; Far, J.; Kune, C.; Larriba-Andaluz, C.; Delaude, L.; Pauw, E. D. *Dalton Trans.* **2016**, *45*, 6361-6370.

(57) Fiedler, T.; Chen, L.; Wagner, N. D.; Russell, D. H.; Gladysz, J. A. *Organometallics* **2016**, *35*, 2071-2075.

(58) Song, L.-J.; Wang, T.; Zhang, X.; Chung, L. W.; Wu, Y.-D. *ACS Catal.* **2017**, *7*, 1361-1368.

(59) More recently, trapped ion mobility spectrometry has been applied for the investigation of cationic organometallic gold complexes: Greisch, J.-F.; Weis, P.; Brendle, K.; Kappes, M. M.; Haler, J. R. N.; Far, J.; De Pauw, E.; Albers, C.; Bay, S.; Wurm, T.; Rudolph, M.; Schulmeister, J.; Hashmi, A. S. K. *Organometallics* **2018**, *37*, 1493-1500.

(60) Inoue, A.; Kitagawa, K.; Shinokubo, H.; Oshima, K. *J. Org. Chem.* **2001**, *66*, 4333-4339.

(61) Schnegelsberg, C.; Bachmann, S.; Kolter, M.; Auth, T.; John, M.; Stalke, D.; Koszinowski, K. *Chem. Eur. J.* **2016**, *22*, 7752-7762.

(62) Parchoymk, T.; Demeshko, S.; Meyer, F.; Koszinowski, *J. Am. Chem. Soc.* **2018**, *140*, 9709-9720.

(63) Neidig, M. L.; Carpenter, S. H.; Curran, D. J.; DeMuth, J. C.; Fleischauer, V. E.; Iannuzzi, T. E.; Neate, P. G. N.; Sears, J. D. *Acc. Chem. Res.* **2019**, *52*, 140-150.

(64) Amatore, C.; Jutand, A. *Acc. Chem. Res.* **2000**, *33*, 314-321.

(65) Terao, J.; Kambe, N. *Acc. Chem. Res.* **2008**, *41*, 1545-1554.

(66) Kolter, M.; Böck, K.; Karaghiosoff, K. Koszinowski, K. *Angew. Chem. Int. Ed.* **2017**, *56*, 13244-13248.

(67) Kolter, M.; Koszinowski, K. *Chem. Eur. J.* **2019**, *25*, 13376-13384.

(68) Lipshutz, B. H.; Keith, J.; Buzard, D. J. *Organometallics* **1999**, *18*, 1571-1574.

(69) Putau, A.; Koszinowski, K. *Organometallics* **2010**, *29*, 3593-3601; Addition/Correction: ibid. **2010**, *29*, 6841-6842.

(70) Putau, A.; Wilken, M.; Koszinowski, K. *Chem. Eur. J.* **2013**, *19*, 10992-10999.

(71) Trefz, T. K.; Henderson, M. A.; Linnolahti, M.; Collins, S.; McIndoe, J. S. *Chem. Eur. J.* **2015**, *21*, 2980-2991.

(72) Zijlstra, H.; Collins, S.; McIndoe, J. S. *Chem. Eur. J.* **2018**, 24, 5506-5512.

(73) Wittig, G.; Raff, P. *Justus Liebigs Ann. Chem.* **1951**, *573*, 195-209.

(74) Holzapfel, H.; Richter, C. *J. Prakt. Chem.* **1964**, *4*, 15-23.

(75) Damico, R. *J. Org. Chem.*, **1964**, *29*, 1971-1976.

(76) Tochtermann, W. *Angew. Chem. Int. Ed. Engl.* **1966**, *5*, 351-371.

(77) Auth, T.; Koszinowski, K.; O'Hair, R. A. J. *Organometallics* **2020**, *39*, 25-33.

(78) Alaviuhkola, T.; Bobacka, J.; Nissinen, M.; Rissanen, K.; Ivaska, A.; Pursiainen, J. *Chem. Eur. J.* **2005**, 11, 2071-2080.

(79) Yakelis, N. A.; Bergman, R. G. *Organometallics* **2005**, *24*, 3579-3581.

(80) Mason, E. A.; Schamp, H. W. *Ann. Phys.* **1958**, *4*, 233-270.

(81) Allen, S. J.; Giles, K.; Gilbert, T.; Bush, M. F. Analyst **2016**, *141*, 884-891.

(82) Adamo, C.; Barone, V. *J Chem. Phys.* **1999**, *110*, 6158-6170.

(83) *Gaussian 09*, revision D.01; Gaussian, Inc.: Wallingford, CT, 2013.

(84) *NBO*, version 3.1; University of Wisconsin: Madison, WI, 1995.

(85) Grimme, S.; Antony, J.; Ehrlich, S.; Krieg, H. *J Chem. Phys.* **2010**, *132*, 154104.

(86) Grimme, S.; Ehrlich, S.; Goerigk, L. *J. Comput. Chem.* **2011**, *32*, 1456-1465.

(87) Weigend, F.; Ahlrichs, R. *Phys. Chem. Chem. Phys.* **2005**, *7*, 3297-3305.

(88) Dolg, M.; Wedig, U.; Stoll, H.; Preuss, H. *J. Chem. Phys.* **1987**, *86*, 866-872.

(89) Andrae, D.; Häußermann, U.; Dolg, M.; Stoll, H.; Preuß, H. *Theor. Chim. Acta* **1990**, *77*, 123-141.

(90) Reed, A. E.; Weinstock, R. B.; Weinhold, F. *J Chem. Phys.* **1985**, *83*, 735-746.

(91) Singh, U. C.; Kollman, P. A. *J. Comput. Chem.* **1984**, *5*, 129-145.

(92) Grimme, S. *Chem. Eur. J.* **2012**, *18*, 9955-9964.

(93) von Helden, G.; Hsu, M. T.; Gotts, N.; Bowers, M. T. *J. Phys. Chem.* **1993**, *97*, 8182-8192.

(94) Shvartsburg, A. A.; Jarrold, M. F. *Chem. Phys. Lett.* **1996**, *261*, 86-91.

(95) Mesleh, M. F.; Hunter, J. M.; Shvartsburg, A. A.; Schatz, G. C.; Jarrold, M. F. *J. Phys. Chem.* **1996**, *100*, 16082-16086; Addition/Correction: *J. Phys. Chem. A* **1997**, *101*, 968.

(96) Kim, H.; Kim, H. I.; Johnson, P. V.; Beegle, L. W.; Beauchamp, J. L.; Goddard, W. A.; Kanik, I. *Anal. Chem.* **2008**, *80*, 1928-1936.

(97) Aggregate formation/detection increased with increasing salt concentration. Dependent on the organyl group R of the borates, n_{max} of the observed $[Na_{n-1}(BR_4)_n]^-$ ions increased in the order of Et < bPh < Xy <Ph.

(98) In the case of $[Na_{n-1}(BPh_4)_n]^-$, where $^{DT}CCS_{He}$ values for n = 1–10 could be determined, the linear growth trend only holds for n = 1–6.

(99) Bleiholder, C.; Dupuis, N. F.; Wyttenbach, T.; Bowers, M. T. *Nat. Chem.* **2011**, *3*, 172-177.

(100) Do, T. D.; de Almeida, N. E. C.; LaPointe, N. E.; Chamas, A.; Feinstein, S. C.; Bowers, M. T. *Anal. Chem.* **2016**, *88*, 868-876.

(101) The BPh_4^- affinity of $[Li(BPh_4)]$ has been calculated to be 155 kJ mol^{-1} in ref. 77. Therefore, it is not unexpected that $[Li_{n-1}(BPh_4)_n]^-$ species with $n > 2$ are not generally accessible under the energetic conditions of ESI mass spectrometry.

(102) Mantina, M.; Chamberlin, A. C.; Valero, R.; Cramer, C. J.; Truhlar, D. G. *J. Phys. Chem. A* **2009**, *113*, 5806-5812.

(103) Behrens, U.; Hoffmann, F.; Olbrich, F. *Organometallics* **2012**, *31*, 905-913.

(104) Grimme, S.; Brandenburg, J. G.; Bannwarth, C.; Hansen, A. *J. Chem. Phys.* **2015**, *143*, 054107.

(105) Siu, C.-K.; Guo, Y.; Saminathan, I. S.; Hopkinson, A. C.; Siu, K. W. M. *J. Phys. Chem. B* **2010**, *114*, 1204-1212.

(106) Campuzano, I.; Bush, M. F.; Robinson, C. V.; Beaumont, C.; Richardson, K.; Kim, H.; Kim, H. I. *Anal. Chem.* **2012**, *84*, 1026-1033.

(107) Lee, J. W.; Davidson, K. L.; Bush, M. F.; Kim, H. I. *Analyst* **2017**, *142*, 4289-4298.

(108) Lee, J. W.; Lee, H. H. L.; Davidson, K. L.; Bush, M. F.; Kim, H. I. *Analyst* **2018**, *143*, 1786-1796.

(109) Ieritano, C.; Crouse, J.; Campbell, J. L.; Hopkins, W. S. *Analyst* **2019**, *144*, 1660-1670.

(110) Alternatively, the *CCS* values of anionic species can be calculated with the SEDI method: Shvartsburg, A. A.; Liu, B.; Jarrold, M. F.; Ho, K.-M. *J. Chem. Phys.* **2000**, *112*, 4517-4526.

(111) TM calculations featuring a scaling factor for x_C' in the range of 0.9–1.1 together with a scaling factor for D_C' that was optimized on the basis of the results for $[Na(BPh_4)_2]^-$ for the given x_C' scaling factor all yielded very similar agreement between the $^{DT}CCS_{N2}$ and $^{TM}CCS_{N2}$ values for the tetraorganylborate species.

(112) $CsBPh_4$ was chosen, because Cs^+ corresponds to the largest alkali metal ion of those considered and thus, goes along with the formation of complementary tetraorganylborate aggregates, as they differ most with respect to their *CCS*s from the sodium-bound analogues.

(113) Referring to ref. 45 and 114, deviations up to 2% of $^{TW}CCS_{N2}$ from $^{DT}CCS_{N2}$ values correspond to the expectation in the case of matched analyte and calibrant ions.

(114) Hinnenkamp, V.; Klein, J.; Meckelmann, S. W.; Balsaa, P.; Schmidt, T. C.; Schmitz, O. J. *Anal. Chem.* **2018**, *90*, 12042-12050.

(115) For the $[Ag_nPh_{n+1}]^-$ ions, the same conclusion has very recently been reached in a gas-phase UV-ion spectroscopy study: Daly, S.; Weske, S.; Mravak, A.; Krstić, M.; Kulesza, A.; Antoine, A.; Bonačić-Koutecký, Dugourd, P.; Koszinowski, K.; O'Hair, R. A. J. *J. Chem. Phys.* **2021**, *154*, 224301.

(116) Hope, H.; Olmstead, M. M.; Power, P. P.; Sandell, J.; Xu, X. *J. Am. Chem. Soc.* **1985**, *107*, 4337–4338.

(117) Röhr, M. I. S.; Petersen, J.; Brunet, C.; Antoine, R.; Broyer, M.; Dugourd, P.; Bonačić-Koutecký, V.; O'Hair, R. A. J.; Mitrić, R. *J. Phys. Chem. Lett.* **2012**, *3*, 1197-1201.

(118) Edwards, P. G.; Gellert, R. W.; Marks, M. W.; Bau, R. *J. Am. Chem. Soc.* **1982**, *104*, 2072-2073.

(119) Hope, H.; Oram, D.; Power, P. P. *J. Am. Chem. Soc.* **1984**, *106*, 1149-1150.

(120) Chiang, M. Y.; Bohlen, E.; Bau, R. *J. Am. Chem. Soc.* **1985**, *107*, 1679-1681.

For Table of Contents Only